

Three Dimensional Seminumerical Model to Study Heat Flow in Peripheral Layers of Elliptical Shaped Human Limbs

Mamta Agrawal

Department of Mathematics, Maulana Azad National Institute
of Technology, Bhopal, 462051, India
mamta_agrawal2311@yahoo.co.in

Neeru Adlakha

Department of Mathematics, SVNIT, Surat, India

K. R. Pardasani

Department of Mathematics, Maulana Azad National Institute
of Technology, Bhopal, 462051, India

Abstract

A number of attempts have been made to study heat flow in circular cross-section of human limbs. But almost no attempt has been reported in literature about study of heat flow in the tissue layers of elliptical shaped human limbs. Therefore, a seminumerical model has been developed to study heat flow in peripheral layers of three-dimensional elliptical shaped human limbs for a steady state case. Appropriate variation in parameters like blood mass flow rate, metabolic activity and thermal conductivity has been incorporated in the model. Appropriate boundary conditions have been framed based on the assumptions that outer surface of the limbs is exposed to the environment. The finite element method has been employed along radial and angular direction and Fourier series method along axial direction to obtain temperature profiles in the region.

Mathematics Subject Classification: 92C35 , 65L60

Keywords: Variational form, Finite element method, Blood mass flow rate, Metabolic activity and Fourier series

1 Introduction

The skin in human body or animal body is boundary lamina, which plays an important role in temperature regulation. It is composed of three layers namely epidermis, dermis and subcutaneous tissues. There are no blood vessels in the epidermis, so there is no blood flow and metabolic activity in this outermost layer. The density of the blood vessels increases as we go down the dermis and becomes almost uniform in the layer below the dermis namely subdermal tissues. The core of the main trunk of the human remains at almost uniform temperature 37°C by maintaining the balance between heat generation within the body and heat loss from the body, but in limbs the core temperature may vary under changing environmental conditions. The core temperature of the human limbs varies extensively as we move away from the body trunk. This is due to the fact that the arterial blood flows from the trunk at body core temperature to the outer shell, loses heat while moving towards the extremities and returns as a colder venous blood temperature. The core temperature also varies along the angular direction of the limbs. This is because the arteries carrying blood from the trunk to the limbs lie on one side of the limb, while the superficial veins responsible for carrying blood towards the heart, lie on the other side.

Earlier experimental investigations were made by Patterson [1] to obtain temperature profiles in the SST region. Some theoretical investigations have been carried out during the last few decades by Cooper and Trezek [16], Chao et. al. [5] and Saxena [17] to study temperature distribution in SST region under normal environmental and physiological conditions. Also attempts have been made by Pardasani and Adlakha [6] and Jain [15] to study problems involving abnormalities like tumors in SST regions of human body. Some models have been developed by Mitchell et.al [4], Saxena et al. [17],[18], Pardasani and Adlakha [7-9], Zhu et. al [13], Song et al [19] and Pardasani and Jas [14] for temperature variation in human limbs for one, two and three dimensional steady state cases by using several techniques like finite element method, Ritz method and pseudo analytical approaches etc. under normal physiological and environmental conditions. Also Shakya [10],[11] has extended finite element modeling to infinite domains.

From the above literature survey, it is evident that all the research workers have assumed that human limb is perfectly circular in shape. But actually human limb is not perfectly circular in shape, it may be considered as elliptical in shape. So for realistic studies, it becomes necessary to develop a three dimensional model to study the radial, angular and axial temperature distribution in dermal regions of human limbs which are elliptical in shape. The semi-numerical approach which consists of a combination of finite element method [3] and Fourier series [2] has been employed to obtain the numerical results.

2 Mathematical Model

The mathematical model given by Perl [20] for temperature distribution in living tissues for a three-dimensional steady state case in elliptical coordinates may be written as :

$$\frac{1}{d^2(\sinh^2 \mu + \sin^2 \nu)} \left[K \frac{\partial}{\partial \mu} \left(\frac{\partial T}{\partial \mu} \right) + K \frac{\partial}{\partial \nu} \left(\frac{\partial T}{\partial \nu} \right) \right] + K \frac{\partial}{\partial z} \left(\frac{\partial T}{\partial z} \right) + M(T_A - T) + S = 0. \tag{1}$$

Where, d is the Eccentricity of elliptical layer, K is the Thermal conductivity, M is the Blood mass flow, S is the Metabolic heat and T_A is the Arterial blood temperature . Here, μ , ν and z are respectively radial, angular and axial coordinates for the elliptical shaped human limbs. The outer surface of the limb is exposed to the environment and heat loss at this surface takes place due to conduction, convection, radiation and evaporation which is given as:

$$-K \frac{\partial T}{\partial \eta} \Big|_{\mu=\mu_3} = h(T - T_a) + LE. \tag{2}$$

Here, h is the heat transfer coefficient, T_a is the atmospheric temperature, L is the Latent heat, and E is the rate of sweat evaporation. The blood moves in arteries from the trunk at body core temperature i.e. $37^{\circ}C$ into the limbs. This blood loses heat to the tissues while moving towards the extremities of the limbs. Thus the blood is at a lower temperature at extreme parts of the limbs. So the inner core temperature of the limb has been taken to be variable along the axial direction of the limb. Hence the following boundary conditions are imposed at the inner boundary [4]:

$$T(\mu_0, \nu, z) = G_{11} + G_{12}e^{-\xi z} \tag{3}$$

$$T_0(\nu, z) = T_{0a}(\nu) \quad \text{at } z = a \quad \text{and} \quad T_0(\nu, z) = T_{0b}(\nu) \quad \text{at } z = b \tag{4}$$

The constants G_{11} and G_{12} are obtained by using above conditions and eqn.(4). The two opposite sides of the inner core of the limb may be at different temperatures, so at the two ends of the limb the following parabolic variation of the core temperature along angular direction has been taken [14]:

$$T_{0a}(\nu) = C_{1a} + C_{2a}\nu + C_{3a}\nu^2 \tag{5}$$

$$T_{0b}(\nu) = C_{1b} + C_{2b}\nu + C_{3b}\nu^2 \tag{6}$$

such that,

$$\begin{aligned} T_{0a}(\nu) &= T_{a0} & \text{at } \nu &= 0 \\ T_{0a}(\nu) &= T_{a\pi} & \text{at } \nu &= \pi \\ T_{0a}(\nu) &= T_{a0} & \text{at } \nu &= 2\pi \end{aligned} \tag{7}$$

$$\begin{aligned}
 T_{0b}(\nu) &= T_{b0} & \text{at } \nu &= 0 \\
 \text{and, } T_{0b}(\nu) &= T_{b\pi} & \text{at } \nu &= \pi \\
 T_{0b}(\nu) &= T_{b0} & \text{at } \nu &= 2\pi
 \end{aligned}
 \tag{8}$$

The constants $C_{1a}, C_{2a}, C_{3a}, C_{1b}, C_{2b}$ and C_{3b} in equation (5) and equation (6) are obtained by using above conditions (7) and (8). The temperature distribution in the limbs will be uniform along z-direction near the trunk whereas the core temperature is uniform up to small distances. The other extremity of the limbs is assumed to be perfectly insulated and no heat loss takes place along the z-direction to the environment. Thus the flux along the z-direction at both the ends of the limbs is assumed to be zero as given below:

$$\frac{\partial T}{\partial z} = 0 \quad \text{at } z = a \tag{9}$$

$$\frac{\partial T}{\partial z} = 0 \quad \text{at } z = b \tag{10}$$

Since the radial distances are very small as compared to the axial distances, so the gradients at the two extremities of the limbs will be negligible. Also the thermoregulation process tries to preserve the heat by insulation and make up the heat loss by heat generation, thus reducing the temperature gradients to maintain the thermal balance. Now, the dermal region of the limb has been divided into three concentric elliptical layers with inner and outer distances μ_0 and μ_3 respectively, the outermost layer is the epidermis. Below the epidermis is the dermis followed by a layer of subdermal tissues. The innermost solid part is the limb core consisting of bone, muscles, large blood vessels etc. These layers have been further discretized into subregions i.e. into twenty-four elements of elliptical sectors with two of its sides curved along angular direction. The angular points of each element are the nodes (see Fig.1). The element information is given in table 1. The equation (1) and equation (2) are transformed into the following discretized variational form [12] for the e^{th} element :

$$\begin{aligned}
 I^{(e)} &= \frac{1}{2} \int_{\in 1} \left[\begin{aligned} &K^{(e)} \left\{ \left(\frac{\partial T^{(e)}}{\partial \mu} \right)^2 + \left(\frac{\partial T^{(e)}}{\partial \nu} \right)^2 + A_1^{(e)} \frac{\partial^2}{\partial z^2} (T^{(e)})^2 \right\} + A_1^{(e)} \\ &M^{(e)} \left(T_A^{(e)} - T^{(e)} \right)^2 - 2A_1^{(e)} S^{(e)} T^{(e)} \end{aligned} \right] d\mu d\nu \\
 &+ \frac{\lambda^{(e)}}{2} \int_{\in 2} A_1^{(e)} [h(T^{(e)} - T_a)^2 + 2LE T^{(e)}] d\nu
 \end{aligned}
 \tag{11}$$

Where, $A_1^{(e)} = d^{(e)2}(\sinh^2 \mu^{(e)} + \sin^2 \nu^{(e)})$ and $e= 1, 2, \dots, 24$. Here, $(\lambda^{(e)} = 1)$ is only for those elements which are exposed to the environment and $\lambda^{(e)} = 0$, for the remaining elements. Also for each sector of elements the arterial temperature $T_A^{(e)}$ is taken to be equivalent to the core temperature on the inner boundary. Hence, we have

$$T_A^{(e)} = T(\mu_0, \nu, z) \tag{12}$$

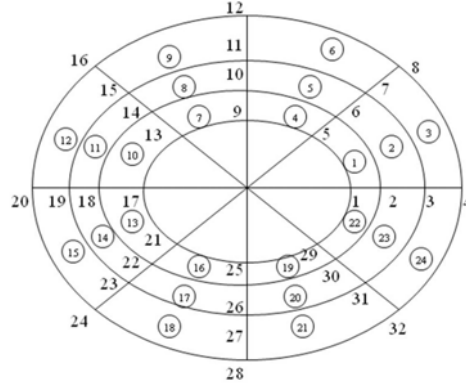


Figure 1: Finite Element discretization of human limb using coaxial elliptical sectoral elements.

Since the thickness of the layers in the SST region is very small so the following linear variation with respect to position along radial direction is assigned to the thermal conductivity, blood mass flow rate and metabolic heat generation in each layer:

$$K^{(e)} = \alpha_1^{(e)} + \alpha_2^{(e)}\mu \ , \ M^{(e)} = \beta_1^{(e)} + \beta_2^{(e)}\mu \ \text{and} \ S^{(e)} = \lambda_1^{(e)} + \lambda_2^{(e)}\mu$$

Where, $\alpha_1^{(e)}$, $\alpha_2^{(e)}$, $\beta_1^{(e)}$, $\beta_2^{(e)}$, $\lambda_1^{(e)}$ and $\lambda_2^{(e)}$ are given below

Subcutaneous tissues e = 1,4,7,10, 13,16,19,22

$$\alpha_1^{(e)} = K_1 \ , \ \alpha_2^{(e)} = 0 \ , \ \beta_1^{(e)} = M_1 \ , \ \beta_2^{(e)} = 0 \ , \ \gamma_1^{(e)} = S_1 \ , \ \gamma_2^{(e)} = 0,$$

Dermis e = 2,5,8,11,14,17,20,23

$$\alpha_1^{(e)} = \frac{K_1\mu_2 - K_3\mu_1}{\mu_2 - \mu_1} \ , \ \alpha_2^{(e)} = \frac{K_3 - K_1}{\mu_2 - \mu_1} \ , \ \beta_1^{(e)} = \frac{M_1\mu_2 - M_3\mu_1}{\mu_2 - \mu_1}$$

$$\beta_2^{(e)} = \frac{M_3 - M_1}{\mu_2 - \mu_1} \ , \ \gamma_1^{(e)} = \frac{S_1\mu_2 - S_3\mu_1}{\mu_2 - \mu_1} \ , \ \gamma_2^{(e)} = \frac{S_3 - S_1}{\mu_2 - \mu_1}$$

Epidermis e = 3,6,9,12,15,18,21, 24

$$\alpha_1^{(e)} = K_3 \ , \ \alpha_2^{(e)} = 0 \ , \ \beta_1^{(e)} = 0 \ , \ \beta_2^{(e)} = 0 \ , \ \gamma_1^{(e)} = 0 \ , \ \gamma_2^{(e)} = 0.$$

The following bilinear shape function for the variation of temperature within each element has been taken as:

$$T^{(e)} = \xi_1^{(e)} + \xi_2^{(e)}\mu + \xi_3^{(e)}\nu + \xi_4^{(e)}\mu\nu \tag{13}$$

Where, $\xi_1^{(e)}$, $\xi_2^{(e)}$, $\xi_3^{(e)}$ and $\xi_4^{(e)}$ are constants for the e^{th} element. The expression in equation (13) in matrix notation can be written as:

$$T^{(e)} = P^T \xi^{(e)} \tag{14}$$

Where, $P^T = [1 \quad \mu \quad \nu \quad \mu\nu]$ and $(\xi^{(e)})^T = [\xi_1^{(e)} \quad \xi_2^{(e)} \quad \xi_3^{(e)} \quad \xi_4^{(e)}]$
Using nodal conditions we get,

$$T(\mu_\eta, \nu_\eta, z_\eta) = T_\eta; \quad \text{Where } \eta = i, j, k, l \quad (15)$$

From equation (14) and equation (15) we get,

$$\bar{T}^{(e)} = P^{(e)} \xi^{(e)} \quad (16)$$

$$\text{Where, } \bar{T}^{(e)} = \begin{bmatrix} T_i \\ T_j \\ T_k \\ T_l \end{bmatrix} \quad \text{and } P^{(e)} = \begin{bmatrix} 1 & \mu_i & \nu_i & \mu_i \nu_i \\ 1 & \mu_j & \nu_j & \mu_j \nu_j \\ 1 & \mu_k & \nu_k & \mu_k \nu_k \\ 1 & \mu_l & \nu_l & \mu_l \nu_l \end{bmatrix}$$

From equation (16) we have,

$$\xi^{(e)} = R^{(e)} \bar{T}^{(e)} \quad (17)$$

where,

$$R^{(e)} = P^{(e)-1}.$$

Substituting $\xi^{(e)}$ from equation (17) in equation (14) we get,

$$T^{(e)} = P^T R^{(e)} \bar{T}^{(e)} \quad (18)$$

Now, the integral $I^{(e)}$ given in equation (11) can be put in the form

$$I^{(e)} = I_k^{(e)} + I_m^{(e)} - I_s^{(e)} + I_\lambda^{(e)} + I_\mu^{(e)} \quad (19)$$

Where,

$$I_k^{(e)} = \frac{1}{2} \int_{\nu_i}^{\nu_k} \int_{\mu_i}^{\mu_j} K^{(e)} \left[\left(\frac{\partial T^{(e)}}{\partial \mu} \right)^2 + \left(\frac{\partial T^{(e)}}{\partial \nu} \right)^2 \right] d\mu d\nu \quad (20)$$

$$I_m^{(e)} = \frac{1}{2} \int_{\nu_i}^{\nu_k} \int_{\mu_i}^{\mu_j} A_1^{(e)} M^{(e)} \left[T_A^{(e)2} + T^{(e)2} \right] d\mu d\nu \quad (21)$$

$$I_{(s)}^{(e)} = \int_{\nu_i}^{\nu_k} \int_{\mu_i}^{\mu_j} A_1^{(e)} \left[M^{(e)} T_A^{(e)} + S^{(e)} \right] T^{(e)} d\mu d\nu \quad (22)$$

$$I_{(\lambda)}^{(e)} = \frac{\lambda^{(e)}}{2} \int_{\nu_j}^{\nu_l} A_1^{(e)} \left[h (T^{(e)} - T_a)^2 + 2 LE T^{(e)} \right] d\nu \quad |_{\mu=\mu_3} \quad (23)$$

$$I_\mu^{(e)} = \frac{1}{2} \int_{\mu_i}^{\mu_j} K^{(e)} A_1 \frac{\partial^2}{\partial z^2} (T^{(e)})^2 d\mu. \quad (24)$$

Now putting value of $T^{(e)}$ from equation (18) in equations (20), (21), (22), (23) and (24) and then minimizing with respect to each nodal point temperature

with the assumption that the parameters $K^{(e)}$, $M^{(e)}$ and $S^{(e)}$ are constants but different in each layer, we get:

$$\frac{dI_k^{(e)}}{d\bar{T}^{(e)}} = \bar{A}^{(e)} \bar{T}^{(e)}, \quad \frac{dI_m^{(e)}}{d\bar{T}^{(e)}} = B^{(e)} \bar{T}^{(e)} \tag{25}$$

$$\frac{dI_s^{(e)}}{d\bar{T}^{(e)}} = G^{(e)}, \quad \frac{dI_\lambda^{(e)}}{d\bar{T}^{(e)}} = F^{(e)} \bar{T}^{(e)} + D^{(e)} \tag{26}$$

$$\frac{dI_\mu^{(e)}}{d\bar{T}^{(e)}} = H^{(e)} \frac{d^2 \bar{T}^{(e)}}{dz^2} \tag{27}$$

Where, $\bar{A}^{(e)} = R^{(e)T} [\bar{A}_{ij}]_{4 \times 4} R^{(e)}$, $B^{(e)} = R^{(e)T} [B_{ij}]_{4 \times 4} R^{(e)}$,
 $G^{(e)} = R^{(e)T} [G_i]_{4 \times 1}$, $F^{(e)} = R^{(e)T} [F_{ij}]_{4 \times 4} R^{(e)}$
 $D^{(e)} = R^{(e)T} [D_i]_{4 \times 1}$ and $H^{(e)} = R^{(e)T} [H_{ij}]_{4 \times 4} R^{(e)}$.
 Here, $\bar{A}_{ij}, B_{ij}, F_{ij}, H_{ij}$ ($i, j=1,2,3, 4$) and G_i, D_i ($i=1,2,3,4$) are constants.
 Now, from equation (19) we have following equation:

$$\frac{dI^{(e)}}{d\bar{T}^{(e)}} = \frac{dI_k^{(e)}}{d\bar{T}^{(e)}} + \frac{dI_m^{(e)}}{d\bar{T}^{(e)}} - \frac{dI_s^{(e)}}{d\bar{T}^{(e)}} + \frac{dI_\lambda^{(e)}}{d\bar{T}^{(e)}} + \frac{dI_\mu^{(e)}}{d\bar{T}^{(e)}} \tag{28}$$

On putting values of equations (25), (26) and (27) in equation (28) we get,

$$\frac{dI}{d\bar{T}} = \sum_{e=1}^N \bar{M}^{(e)} \frac{dI^{(e)}}{d\bar{T}^{(e)}} \bar{M}^{(e)T} \tag{29}$$

Where, $\bar{M}^{(e)} = \begin{bmatrix} 0 & 0 & 0 & 0 \\ \cdot & \cdot & \cdot & \cdot \\ 1 & 0 & 0 & 0 \\ 0 & 1 & 0 & 0 \\ 0 & 0 & 1 & 0 \\ 0 & 0 & 0 & 1 \\ \cdot & \cdot & \cdot & \cdot \\ 0 & 0 & 0 & 0 \end{bmatrix}$ $i^{th} row$
 $j^{th} row$
 $k^{th} row$
 $l^{th} row$ and $I = \sum_{e=1}^{24} I^{(e)}$

The integral I is extremized with respect to each nodal temperature T_i ($i=1,2.. 32$) to obtain a following set of differential equations in terms of nodal temperatures T_i .

$$\bar{X} \bar{T} - \bar{V} \frac{d^2 \bar{T}}{dz^2} = \bar{Y}. \tag{30}$$

Where, \bar{X} and \bar{V} are matrices of order (32 X 32) and \bar{Y} is a matrix. of order (32 X 1).

Also, $\bar{X} = \sum_{e=1}^N \bar{M}^{(e)} [\bar{A}^{(e)} + H^{(e)} + F^{(e)}] \bar{M}^{(e)T}$, $\bar{T} = [T_1 T_2 \dots T_N]^T$

$$\bar{Y}^T = \sum_{e=1}^N \bar{M}^{(e)} [G^{(e)} - D^{(e)}] \text{ and } \bar{V} = \sum_{e=1}^N \bar{M}^{(e)} B^{(e)} \bar{M}^{(e)T}.$$

Here, T_N denotes the N^{th} nodal temperature and N is the number of nodal points. Now, following Fourier series is applied to eliminate the variable z from the above equation (30):

$$T_0 = A_{00} + \sum_{n=1}^{\text{inf}} A_{n0} \cos n\alpha z \quad (31)$$

$$T_i = A_{0i} + \sum_{n=1}^{\text{inf}} A_{ni} \cos n\alpha z \quad (32)$$

Where, $\alpha = \pi/b$ and the coefficients A_{00} and A_{n0} are known due to boundary condition (3). All coefficients A_{0i} and A_{ni} are obtained by solving the following system of linear equations obtained from equations (30), (31) and (32).

$$X^{(1)} A_0 = p^{(1)} \quad (33)$$

$$X^{(2)} A_n = p^{(2)} \quad (34)$$

Where $X^{(v)}$ ($v=1, 2$) are square matrices of order (32 X 32). A_0 and A_n are column matrices of order (32 X 1) and they represent the matrices of coefficients A_{0i} and A_{ni} respectively. $p^{(\sigma)}$ ($\sigma = 1, 2$) is column matrices of order (32 X 1). A computer program has been developed for the entire problem and executed on core 2 duo to compute temperature profiles in each subregion.

3 Results and Discussion

The results have been computed for the atmospheric temperature $T_a = 15^{\circ}\text{C}$ and $E = 0$. The values of the parameters are shown below [18].

$$M_1 = 0.003 \text{ Cal/cm}^3 - \text{min. deg. C}, \quad S_1 = 0.0357 \text{ Cal/cm}^3 - \text{min.}$$

$$K_1 = 0.06 \text{ cal/cm} - \text{min. deg. C}, \quad K_2 = 0.045 \text{ cal/cm} - \text{min. deg. C},$$

$$K_3 = 0.03 \text{ cal/cm} - \text{min. deg. C},$$

$$L = 579.0 \text{ cal/gm}, \quad h = 0.009 \text{ Cal/cm}^2 - \text{min. deg. C}.$$

The constants a , b , T_{a0} , $T_{a\pi}$, T_{b0} and $T_{b\pi}$ can be assigned any values depending upon the situations under study. As a particular case following values have been used [14]:

$$a = 0\text{cm}, \quad b = 20\text{cm},$$

$$T_{a0} = 37^{\circ}\text{C}, \quad T_{b0} = 33^{\circ}\text{C}, \quad T_{a\pi} = 35^{\circ}\text{C} \text{ and } T_{b\pi} = 30^{\circ}\text{C}.$$

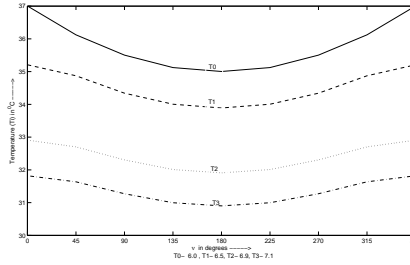


Figure 2: Graph between Temperature and Angle for SET-I at $T_a = 15^{\circ}C$ and $z = a$.

The expression for nodal information is as given below:

$$\text{Radial Coordinates: - } \left. \begin{array}{l} \mu_i = a_0 \quad \text{for } i = 1 + 4j \\ \mu_i = a_1 \quad \quad \quad i = 2 + 4j \\ \mu_i = a_2 \quad \quad \quad i = 3 + 4j \\ \mu_i = a_3 \quad \quad \quad i = 4 + 4j \end{array} \right\} \text{ for } j = 0, 1, 2, \dots, 7$$

$$\text{Angular Coordinates: - } \left. \begin{array}{l} \nu_i = 0 \quad \quad \quad \text{for } i = 1, 2, 3, 4 \\ \nu_{i+4} = \nu_i + 45^{\circ} \quad \text{for } i = 1, 2, 3, \dots, 28 \end{array} \right\}$$

$$\text{Axial Coordinates: - } \left. \begin{array}{l} z_i = a \quad i = 1, 2, \dots, 32 \\ z_{i+32} = b \quad i = 1, 2, \dots, 32 \end{array} \right\}$$

$$\text{Eccentricity is given by: - } \left. \begin{array}{l} d_i = d_0 \quad \quad \quad i = 1 + 4j \\ d_i = d_1 \quad \quad \quad i = 2 + 4j \\ d_i = d_2 \quad \quad \quad i = 3 + 4j \\ d_i = d_3 \quad \quad \quad i = 4 + 4j \end{array} \right\} \text{ for } j = 0, 1, 2, \dots, 7$$

The following set of eccentricity has been taken as a particular case for a sample of limb under study.

$$d_1 = .0030, d_2 = .0020, d_3 = .0017.$$

In above, constants a_i ($i=0,1,2,3$) can be assigned any value depending upon the sample of skin layers under study. Here as a particular case following values have been used [7].

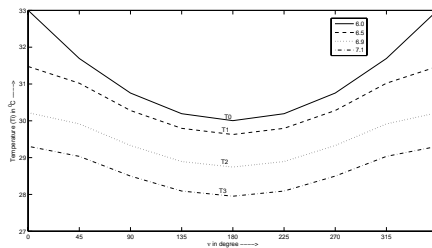
$$\text{SET - I } a_0 = 6.0 \text{ cm}, \quad a_1 = 6.5 \text{ cm}, \quad a_2 = 6.9 \text{ cm}, \quad a_3 = 7.1 \text{ cm}.$$

$$\text{SET - II } a_0 = 6.0 \text{ cm}, \quad a_1 = 6.4 \text{ cm}, \quad a_2 = 6.7 \text{ cm}, \quad a_3 = 6.8 \text{ cm}.$$

The figure-2 and figure-3 represent the variation of temperature along angular direction for $T_a = 15^{\circ}C$, $E = 0$, SET-I, at $z=a$ and $z=b$ respectively. The figure-4 represents the same for SET-II at $z=a$. The profile T_0 in these figures represents the inner boundary condition. The steepness of the curves decreases as we move from the inner core (T_0) towards the outer surface (T_3). This steepness of the profiles is more in figure-3 at $z=b$ as compared to that in figure-2 at $z=a$ due to larger difference in core temperatures at the two opposite ends

| e | i_e | j_e | k_e | l_e |
|----|-------|-------|-------|-------|
| 1 | 1 | 2 | 5 | 6 |
| 2 | 2 | 3 | 6 | 7 |
| 3 | 3 | 4 | 7 | 8 |
| 4 | 5 | 6 | 9 | 10 |
| 5 | 6 | 7 | 10 | 11 |
| 6 | 7 | 8 | 11 | 12 |
| 7 | 9 | 10 | 13 | 14 |
| 8 | 10 | 11 | 14 | 15 |
| 9 | 11 | 12 | 15 | 16 |
| 10 | 13 | 14 | 17 | 18 |
| 11 | 14 | 15 | 18 | 19 |
| 12 | 15 | 16 | 19 | 20 |
| 13 | 17 | 18 | 21 | 22 |
| 14 | 18 | 19 | 22 | 23 |
| 15 | 19 | 20 | 23 | 24 |
| 16 | 21 | 22 | 25 | 26 |
| 17 | 22 | 23 | 26 | 27 |
| 18 | 23 | 24 | 27 | 28 |
| 19 | 25 | 26 | 29 | 30 |
| 20 | 26 | 27 | 30 | 31 |
| 21 | 27 | 28 | 31 | 32 |
| 22 | 29 | 30 | 1 | 2 |
| 23 | 30 | 31 | 2 | 3 |
| 24 | 31 | 32 | 3 | 4 |

Table 1: List of elements used for numerical results

Figure 3: Graph between Temperature and Angle for SET-I at $T_a = 15^{\circ}C$ and $z = b$.

($\nu = 0^{\circ}C$ and $\nu = 180^{\circ}C$) of the cross-section of the limb at $z=b$. Also the gaps between the temperature profiles at $z=a$ for SET-II in figure-4 is less as compared to that in figure-3 for SET-I. This is due to less insulation provided

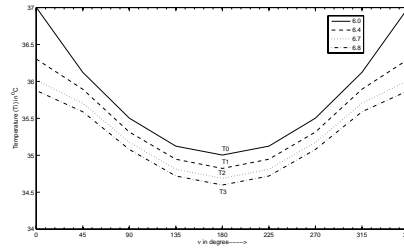


Figure 4: Graph between Temperature and Angle for SET-II at $T_a = 15^{\circ}C$ and $z = a$.

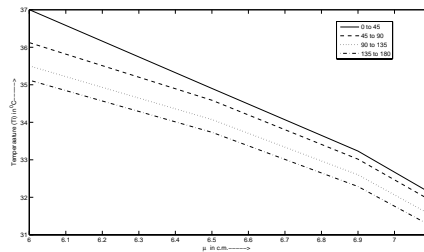


Figure 5: Graph between Temperature and radius for SET-I at $T_a = 15^{\circ}C$ and $z = a$.

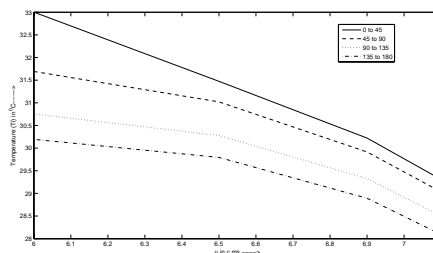


Figure 6: Graph between Temperature and radius for SET-I at $T_a = 15^{\circ}C$ and $z = b$.

by the layers of the SST region of the limb for less thickness. The figure-5 and figure-6 represent the variation of temperature along radial direction for $T_a = 15^{\circ}C$, $E=0$, SET-I at $z=a$ and $z=b$ respectively. The figure-7 and figure-8 represent the variation of temperature along z -direction at $\nu = 0^{\circ}$ and $\nu = 180^{\circ}$ respectively for SET-I. In these figures it can be seen that the temperature is higher near the body trunk ($z=a$) and these temperature profiles fall down as we move towards other end ($z=b$) of the limb. Also the fall in temperature profiles is faster near the trunk and after few centimeters along axial direction the profiles became almost uniform. This is because difference between the core temperature of the limb and the atmospheric temperature

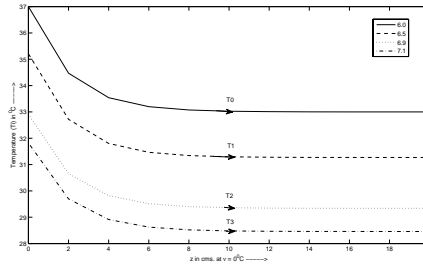


Figure 7: Graph between Temperature and z (in cms.) for SET-I at $T_a = 15^{\circ}C$ and $\nu = 0^{\circ}C$.

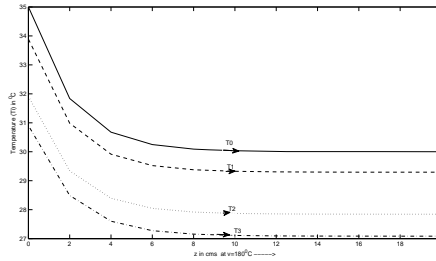


Figure 8: Graph between Temperature and z (in cms.) for SET-I at $T_a = 15^{\circ}C$ and $\nu = 180^{\circ}C$.

decreases as we move towards other end of the limb and is minimum at $z=b$. Moreover the fall in temperature profiles is more in figure-8 at $\nu = 180^{\circ}C$ than in figure-7 at $\nu = 0^{\circ}C$. This is due to larger variation in the core temperature at the two opposite ends of cross-section of the limb at $\nu = 180^{\circ}C$ than at $\nu = 0^{\circ}C$. The numerical results obtained here are in good agreement with those obtained by [8,14]. Also the results obtained here are in agreement with the physiological facts. The seminumerical computational technique; a combination of finite element method and Fourier series employed here has been quite successful in reducing the three dimensional problem further in to two-dimensional problem and obtaining useful results. The computations involved in this method are less as compared to those in variational finite element method for a three dimensional case. Another important feature of this approach is that we have been able to incorporate the realistic geometric shape of the elliptical shaped limb along three dimensions. Thus, the coaxial elliptical sector elements used in this model have provided greater flexibility by making the use of finite element approach easier and reducing the size of computations. With the use of coaxial elliptical sector elements, less number of elements are required to approximate the region as compared to the use of triangular elements. The present model can be further developed and extended to the deep tissues of human limbs where the properties also vary sectorwise

along angular direction, such variations in the physiological parameters can be incorporated with the help of coaxial elliptical sector elements. The approach and model developed here can be useful for application in other problems of engineering and science. Such mathematical models can be developed to obtain thermal information in human organs, which can be of great use to biomedical scientists for clinical applications like development of protocols for diagnosis and therapeutics.

ACKNOWLEDGEMENTS. The authors are highly grateful to Department of Biotechnology, New Delhi, India for providing support in the form of Bioinformatics Infrastructure Facility for carrying out this work.

References

- [1] A.M. Patterson, Measurement of temperature profiles in human skin, *S.Afr.J.Sc.* (1976),72, 78-79.
- [2] G.E. Myers, Analytical methods in conduction heat transfer, McGraw Hill Co., New York,(1971), 320-428.
- [3] J.N. Reddy, An Introduction to the finite element method, McGraw-Hill Book Company, Singapore, (1985),47-52.
- [4] J.W. Mitchell, T. L. Galvez, J. Hengle, G.E. Myers and K.L. Siebercker, Thermal response of human legs during cooling, *J.Appl. Physiology, U.S.A.*, (1970),29 (6), 859-865.
- [5] K.N. Chao, J.G. Easley and W.J. Yang, Heat and water migration in regional skins and subcutaneous tissues, *Bio.Mech. Symp, ASME*,(1973), 69-72.
- [6] K.R. Pardasani and N. Adlakha, Exact solution to a heat flow problem in peripheral tissue layers with a solid tumor in dermis, *Ind.J. Pure.Appl.Math*,(1991), 22(8) 679-682.
- [7] K.R. Pardasani and N. Adlakha, Two-dimensional steady state temperature distribution in annular tissue layers of a human or animal body, *Ind.J.Pure and Appl. Math.*,(1993), 24(11) 721-728
- [8] K.R. Pardasani and N. Adlakha, Coaxial circular sector elements to study two- dimensional heat distribution problem in dermal regions of human limbs. *Mathl.Comput. Modeling*,(1995), Vol.22, No.9, 127-140.

- [9] K.R. Pardasani and N. Adlakha, Coaxial circular sector elements to study radial and angular heat distribution problem in human limbs, Proc. Nat. Acad Sci., India,(1998), 68(A), 1, 55-68.
- [10] K.R. Pardasani. and M. Shakya , Infinite element thermal model for human dermal regions with tumors, Int. Journal of Applied Sc. & Computations, May (2008),Vol. 15, No. 1, pp. 1-10.
- [11] K.R. Pardasani and M. Shakya, Three dimensional infinite element model to study thermal disturbances in human peripheral region due to tumor, J.of Biomechanics, (2006), Vol. 39, Suppl.1, P.S634.
- [12] M.K. Jain, S.R.K. Iyengar and R.K. Jain, Numerical methods for scientific and engineering computation, 3rd edn. Wiley Eastern limited, New Delhi, (1990), 155-159.
- [13] M. Zhu, S. Weinbaum and L.M. Jiji, Heat exchange between unequal counter current vessels asymmetrically embedded in a cylinder with surface convection, Int. J. Heat Mass Transfer,(1990), Vol. No. 10, 2275-2284.
- [14] P. Jas, Finite element approach to the thermal study of malignancies in cylindrical human organs, Ph.D. Thesis, MANIT, Bhopal,(2002).
- [15] R.K. Jain, Temperature distribution in normal and neoplastic tissues during Normothermia and hypothermia in "Thermal characteristics of tumors: Application in detection and treatment", R.K.Jain and Gullino, Nyas, (1980),Vol. 335, 48-62.
- [16] T.E. Cooper and G.J. Trezek, A probe technique for determining the thermal conductivity of tissue, J. Heat Trans. ASME,(1972), 94, 133-140.
- [17] V.P.Saxena And D. Arya, Numerical methods in Thermal Problems, Proc. 1st Int.Conf, Pineridge Press, (U.K), (1979) ,P. 1067.
- [18] V.P.Saxen, a and J.S. Bindra, Pseudo-analytic finite partition approach to temperature distribution problem in human limbs, Int. J. Math. Sciences. ,(1989), Vol. 12, 403- 408.
- [19] W.J. Song, S. Weinbaum, L.M. Jiji and D. Lemons, A combined macro and micro vascular model for whole limb heat transfer, Trans. ASME. J. Bio. Mechanical Engineering ,(1988),Vol. 110, 259-268.
- [20] W. Perl, Heat and matter distribution in body tissues and determination of tissue blood flow by local clearance methods, J.Theo. Biol., (1962), 2, 202-235.

Received: April, 2009